Solid-State NMR Spectroscopy

International Edition: DOI: 10.1002/anie.201602936
German Edition: DOI: 10.1002/ange.201602936

^{19}F NMR Spectroscopy as a Highly Sensitive Method for the Direct Monitoring of Confined Crystallization within Nanoporous Materials

*Karol P. Nartowski, Diksha Malhotra, Lucy E. Hawarden, Juraj Sibik, Dinu Iuga, J. Axel Zeitler, László Fábián, and Yaroslav Z. Khimyak**

Abstract: *The introduction of fluorine into the structure of pharmaceuticals has been an effective strategy for tuning their pharmacodynamic properties, with more than 40 new drugs entering the market in the last 15 years. In this context, ^{19}F NMR spectroscopy can be viewed as a useful method for investigating the host–guest chemistry of pharmaceuticals in nanosized drug-delivery systems. Although the interest in confined crystallization, nanosized devices, and porous catalysts is gradually increasing, understanding of the complex phase behavior of organic molecules confined within nanochambers or nanoreactors is still lacking. Using ^{19}F magic-angle-spinning NMR spectroscopy, we obtained detailed mechanistic insight into the crystallization of flufenamic acid (FFA) in a confined environment of mesoporous silica materials with different pore diameters (3.2–29 nm), providing direct experimental evidence for the formation of a molecular-liquid-like layer besides crystalline confined FFA form I.*

The discovery of mesoporous silica materials opened new areas of science in which the properties of solids can be tuned by their encapsulation in porous confinements that are only a few nanometers in diameter.[1] The unique features of such silica scaffolds, including tailored pore diameters and architectures and large surface areas, which can be chemically functionalized, led to their application in catalysis, gas storage, sensing, protein immobilization, and drug delivery.[2] Furthermore, the engineering of nanocrystals confined within nanosized chambers of controlled pore glasses yielded new crystalline structures, stabilized metastable polymorphs, or helped formulating amorphous drug-delivery systems.[3–5] Although the number of studies aimed at new applications of porous silica materials is rising, there is a considerable lack of molecular-level understanding of the phenomena that govern self-assembly in such systems. For example, ibuprofen, benzoic acid, and lauric acid confined within MCM-41 silica (pore diameter ca. 3–4 nm) have been found to be in a highly mobile state, as liquid-like behavior was observed by solid-state NMR spectroscopy.[6] The high mobility of confined ibuprofen (IBU) was confirmed indirectly by hyperpolarized ^{129}Xe NMR and MAS-PFG NMR spectroscopy (MAS = magic angle spinning, PFG = pulsed field gradient), where two different diffusion coefficients were observed for the guest.[7] Dielectric relaxation spectroscopy studies of IBU/MCM-41 confirmed two different motional regimes for IBU, which were assigned to its populations in the pore voids and at the silica surface; this was corroborated by molecular dynamics simulations.[8] Detailed quantum mechanical modeling of the adsorption of clotrimazole and IBU in porous silica confirmed the very high mobility of these guests at silica surfaces, which is in good agreement with the IR and solid-state NMR spectroscopic data.[9]

As fluorinated pharmaceuticals are currently in the spotlight of drug discovery,[10] it is possible to take advantage of the high sensitivity of ^{19}F nuclei to changes in the local environment to probe the nanoscale organization of such molecules confined in porous hosts.

Herein, we demonstrate that ^{19}F solid-state NMR spectroscopy can be used to detect the presence of confined molecules of the model pharmaceutical (flufenamic acid, FFA) in different environments and motional regimes (Figure 1). By encapsulation of FFA in three different silica scaffolds with pore diameters from 3.2 to 29 nm, we were able to fully control the confined crystallization of FFA form I, gaining mechanistic insight into the self-assembly at different length scales. The combined use of ^{19}F MAS NMR spectroscopy and other characterization methods enabled us to monitor the processes in the confined space in situ.

Using a variety of techniques (N_2 adsorption, PXRD, DSC, solid-state NMR, and THz spectroscopy),[11] we have shown that FFA had been encapsulated inside the pores of the three silica scaffolds by the melt loading method (see the Supporting Information, Section S2). We gradually increased the guest loading to achieve gradual filling of the pores with

[*] K. P. Nartowski, D. Malhotra, Dr. L. E. Hawarden, Dr. L. Fábián, Prof. Y. Z. Khimyak
School of Pharmacy, University of East Anglia
Norwich (UK)
E-mail: Y.Khimyak@uea.ac.uk
Dr. J. Sibik, Dr. J. A. Zeitler
Department of Chemical Engineering and Biotechnology
University of Cambridge, Cambridge (UK)
Dr. D. Iuga
UK 850 MHz Solid-State NMR Facility, Department of Physics
Millburn House, University of Warwick
Coventry CV4 7AL (UK)
Dr. L. E. Hawarden
Current address: Drug Product Science and Technology
Bristol-Myers Squibb
Reeds Lane, Moreton, Merseyside, CH46 1QW (UK)
Dr. J. Sibik
Current address: F. Hoffmann-La Roche A. G.
4070 Basel (Switzerland)
K. P. Nartowski
Current address: Department of Drug Form Technology
Faculty of Pharmacy, Wroclaw Medical University
ul. Borowska 211, 50-556 Wroclaw (Poland)
Supporting information and the ORCID identification numbers for the authors of this article can be found under http://dx.doi.org/10.1002/anie.201602936.

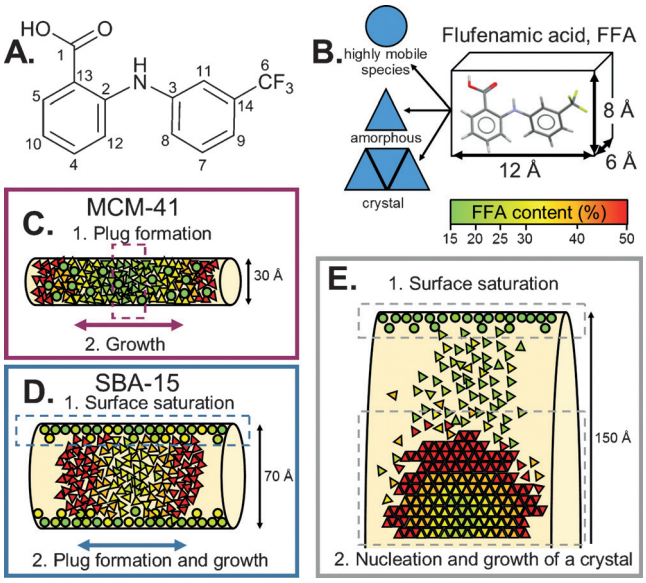

Figure 1. A) Structure of FFA and labeling of the carbon atoms. B) Average dimensions of the FFA molecule and the three different states of FFA species inside the pores. C, D) Different mechanisms for FFA adsorption and stabilization of the amorphous state. E) Mechanism of the formation of crystalline FFA form I in MCF (for a detailed description, see the Supporting Information, Section S3).

different diameters. The materials are labeled as host/FFA X-Y, where the host is MCM-41, SBA-15, or MCF, and X-Y is the host/guest ratio in wt%. It is important to note that stabilization of the extremely unstable amorphous FFA (T_g = 286 K) was achieved for over a year inside the pores of the MCM-41 and SBA-15 hosts.

The encapsulation of organic guest molecules within silica scaffolds leads to either the formation of confined crystals or stabilization of the confined amorphous phase, depending on the properties of the host (mainly the pore size) and the guest molecules (size, flexibility, and thermal behavior). The two outcomes observed for confined FFA were directed primarily by the silica pore size. First, encapsulation in MCM-41 (3.2 nm) or SBA-15 (7.1 nm) results in the stabilization of amorphous FFA across all studied host/guest ratios. No melting point in the DSC thermograms and a broad "halo" in the PXRD traces are characteristic of amorphous solids (see the Supporting Information, Section S5). The crystalline phase detected at high host/guest ratios can be assigned to FFA form I loaded outside the pores, as no decrease or broadening of the melting peak characteristic for confined crystals was observed in DSC.[3a,e,12] The ^{13}C solid-state NMR spectra of the MCM-FFA and SBA-FFA materials show very broad peaks and low signal intensity, especially at low guest contents (see the Supporting Information, Section S5). Such effects characteristic of confined amorphous solids can be attributed to the increased mobility of the guests, reducing the efficiency of ^{1}H–^{13}C cross-polarization.[6c–e]

In contrast to MCM-41 and SBA-15, the formation of crystalline FFA is observed in the pores of MCF silica (pore diameter ca. 29 nm). This effect depended on the loading level of FFA, with the drug remaining amorphous at low loadings (up to 20 wt%) and crystallizing into FFA form I at higher loadings. Crystallization into FFA form I was confirmed by both PXRD and solid-state NMR spectroscopy. The DSC thermograms showed a broadening of the melting peak and a lowering of the melting point of FFA form I, unequivocally confirming the presence of the confined crystalline phase (Figure 2).

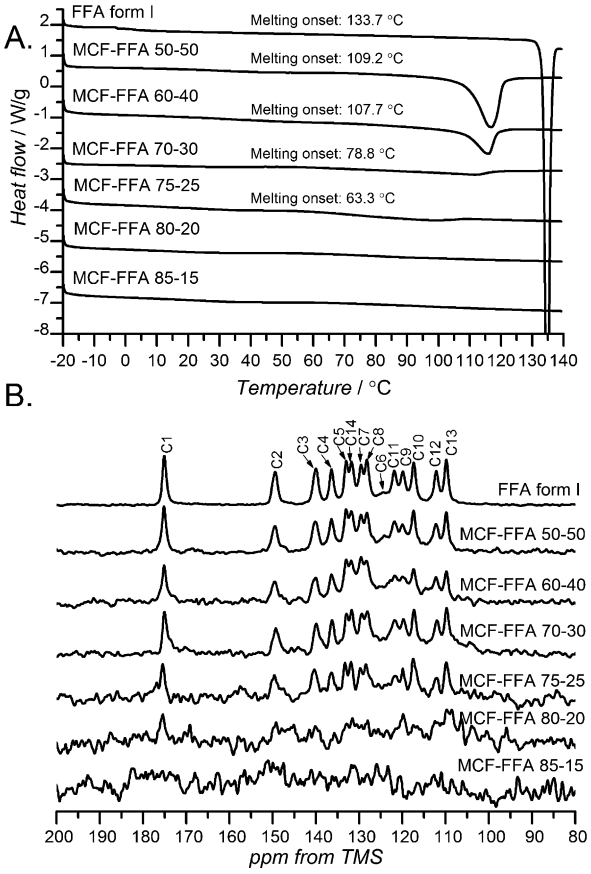

Figure 2. A) DSC thermograms and B) ^{1}H–^{13}C CP/MAS solid-state NMR spectra of MCF loaded with FFA at different host/drug ratios. An increase in the melting onset with increasing drug content (A) indicates a gradual growth of the confined crystal in agreement with the Gibbs–Thomson relationship.[3d,e] For details of the encapsulation methods, see the Supporting Information. The samples were labeled according to the host/FFA ratios (in wt%).

Owing to the high sensitivity of terahertz (THz) spectroscopy to the molecular organization in organic solids, it can be used to show fine differences between bulk and confined FFA.[12,13,14b] Changes in the peak positions and intensities can be observed in the variable temperature (VT) THz spectra of both phases alongside peak broadening for the confined FFA compared to the bulk crystalline material (Figure 3). The blue shifts of the vibrational modes in spectra acquired at the same temperatures for FFA confined in MCF and bulk FFA form I are in line with the previous observations obtained by using waveguide spectroscopy and can be viewed as a further signature of the confinement. The decreased melting point of confined FFA form I is reflected in the loss of the THz signal between 400 and 420 K, which is in agreement with the DSC data. The peak of FFA at 1.6 THz becomes attenuated upon

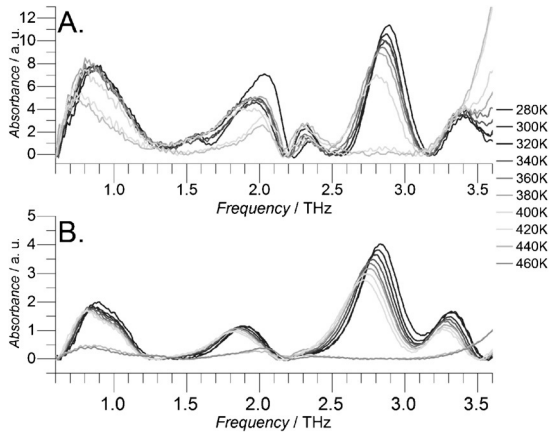

Figure 3. Variable temperature (VT) THz spectra of A) FFA form I confined within MCF (MCF-FFA 60-40) and B) FFA form I. Differences in the peak positions and intensities between bulk and confined FFA form I can be observed for all spectral features. The peak at approximately 2.3 THz is due to the nanoporous silica.

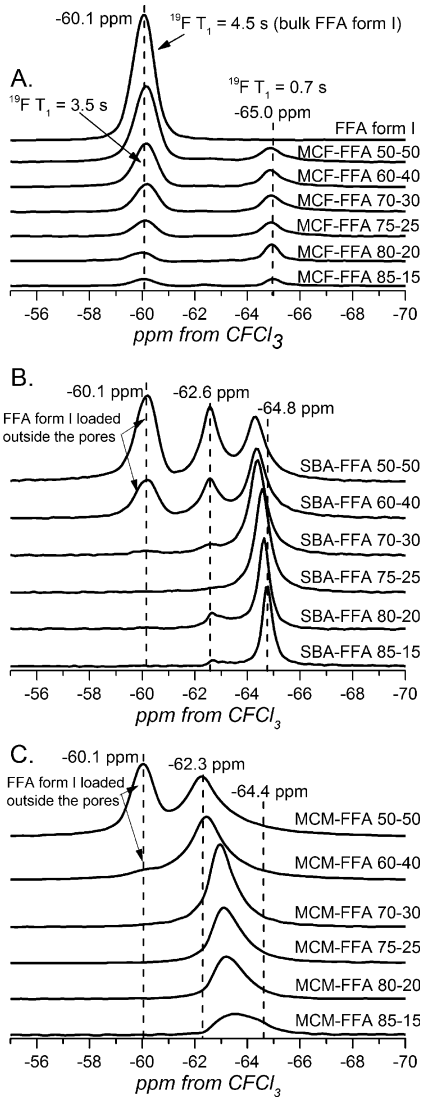

Figure 4. High-field $^{19}F\{^1H\}$ solid-state MAS NMR spectra (20.0 T) of A) MCF-FFA, B) SBA-FFA, and C) MCM-FFA. The samples are labeled according to their host/FFA ratios (in wt%). An increase in the intensities of the main resonances at $\delta = -60$, -62, and -64 ppm with FFA content is consistent with the pore loading pathways indicated in Figure 1 (for details, see the Supporting Information, Section S3). The high-field spectra are in full agreement with the data recorded at 9.4 T (see the Supporting Information, Section S3).

loading FFA into nanopores: this peak is distinct in the low-temperature spectra of pure crystalline FFA, but it is barely visible for FFA confined in MCF (see Figure S15). This highlights the sensitivity of THz spectroscopy towards subtle changes in local ordering: it is exactly this feature that disappears completely upon heating, an effect that is indicative of increased crystalline disorder, which is often due to intramolecular flexibility or rotator phases. It is not surprising that it is this spectral signature that exhibits the most pronounced difference between the bulk and confined FFA as the confinement will limit the degrees of freedom for the FFA molecule to form ordered domains.[14]

Molecules confined within the mesopores of silica materials can be present in several different environments, that is, as confined crystals, amorphous aggregates, or species interacting with the surface of the host. The 100% natural abundance of ^{19}F and its high sensitivity to changes in long-range electrostatic interactions[15] enabled us to detect the differences between these environments for FFA. Advantageously, crystalline FFA form I has one molecule in the asymmetric unit and three magnetically equivalent fluorine atoms in the structure, leading to a single peak at $\delta = -60.1$ ppm in the ^{19}F solid-state NMR spectra recorded at both 9.4 and 20.0 T (Figure 4 A, top spectrum; see also the Supporting Information, Sections S3 and S8).

The ^{19}F solid-state NMR spectra of FFA confined in the MCF host show that the guest species reside in two different environments with the populations depending on the host/guest ratio. A sharp peak at $\delta = -65.0$ ppm is present at the lowest loading. Increasing the FFA content leads to the gradual growth of the broad resonance at $\delta = -60.1$ ppm, attributable to FFA form I (Figure 4), which was also confirmed by ^{13}C NMR spectroscopy (Figure 2). Two additional features of the peak at $\delta = -65.0$ ppm are important for further understanding of the spectra. First, there are no spinning sidebands even at very low MAS rates (1 kHz), indicating very low chemical shift anisotropy (see the Supporting Information, Section S8). This may be related to an increased molecular mobility for this population, which was further corroborated by the ^{19}F T_1 relaxation times (Figure S10). Second, the intensity of this peak showed only minor changes across all host/guest ratios, reaching saturation at 15 wt% FFA. This is in agreement with the expected values for full surface coverage of the pores by a molecular monolayer. The linear increase in the intensity of the peak at approximately $\delta = -60$ ppm (FFA form I) with increasing FFA content indicates the gradual growth of the crystalline phase inside the pores (see the Supporting Information, Sections S2 and S3). Interestingly, it was possible to detect the confined crystalline phase by ^{19}F NMR spectroscopy at loadings as low as 15 wt%, which is below the threshold of

either DSC or PXRD. This may indicate the formation of small nucleating clusters with only local ordering.

The presence of molecules in two distinct environments with different relaxation rates (^{19}F $T_1 \approx 3.5$ s for the confined phase and 0.7 s for the liquid-like surface layer) supports the concept of a highly dynamic liquid-like molecular layer formed on the internal surface of the pores.[9] The presence of the liquid-like FFA layer on the silica surface is not surprising, as host–guest interactions between the hydrophobic FFA guest and the silica surface of the host with a high content of ^{3}Q [$(SiO)_3SiOH$] sites (see the Supporting Information, Section S6) are expected to be weak. Similar phenomena have been suggested by the DFT and MD simulations of ibuprofen and clotrimazole encapsulated in MCM-41 and MSU silica materials.[9] Importantly, these molecules share similar properties with FFA (i.e., hydrophobicity and the presence of a carboxyl group in IBU).

Similarly to MCF-FFA materials, two different environments can be detected for FFA molecules when confined in MCM-41 and SBA-15. For SBA-FFA composites, a peak at $\delta = -64.8$ ppm is observed at low loading levels. An increase in FFA content leads to its downfield shift and the growth of a resonance corresponding to the confined amorphous drug at $\delta = -62.6$ ppm.

The ^{19}F NMR spectra of the MCM-FFA composites show two (merged) peaks at $\delta = -63.5$ and -64.4 ppm, which undergo a downfield shift with increasing drug content. The very low intensity of the spinning sidebands in both SBA-FFA and MCM-FFA with up to 30 wt % of FFA is consistent with the presence of a disordered amorphous guest phase along with the liquid-like layer of FFA, which was also confirmed by the ^{19}F T_1 relaxation times (see the Supporting Information, Sections S3 and S5).

FFA loaded into the MCF host crystallizes into FFA form I after a couple of hours. By using ^{19}F NMR spectroscopy, we monitored the crystallization of MCF-confined FFA form I from the amorphous form in situ. At 293 K, two broad resonances were observed that are due to a highly mobile species of FFA ($\delta = -65$ ppm) alongside amorphous plugs of the drug in the pore voids ($\delta = -62$ ppm). An increase in temperature resulted in the narrowing of both resonances owing to increased mobility. At 323 K, the growth of an additional broad peak of confined FFA form I was observed at $\delta = -60.0$ ppm (Figure 5B). The intensity of this peak during isothermal recrystallization at 333 K reached its maximum after 60 min (Figure 5A). At the same time, the intensity of the resonance of confined amorphous FFA ($\delta = -62.3$ ppm) reached a minimum and subsequently stabilized. Interestingly, there was only a slight change in the intensity of the resonance at $\delta = -65$ ppm, indicating that the population of FFA molecules in the liquid-like layer is practically unaffected by the crystallization. The spectrum acquired at room temperature following the whole recrystallization experiment showed only two lines, namely a broad resonance at approximately $\delta = -60$ ppm (FFA form I) and a sharper resonance at about $\delta = -65$ ppm (highly mobile FFA species). The amorphous SBA-FFA composite shows very different behavior at elevated temperatures (Figure S16). Only two ^{19}F NMR resonances, which narrowed with increasing temperature (up to 333 K), were observed. No crystallization was detected, indicating the effective stabilization of confined amorphous FFA. This was further confirmed by variable-temperature THz spectroscopy (see the Supporting Information, Section S5 and Figure S15).

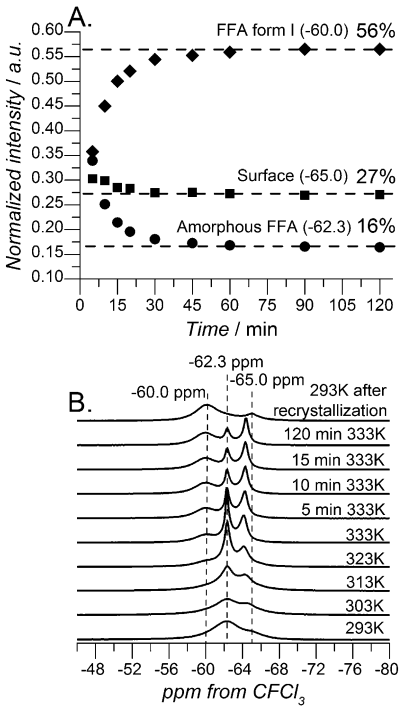

Figure 5. A) Kinetics (333 K) of the confined crystallization of FFA in MCF at a 60-40 host/guest ratio. B) Variable-temperature ^{19}F solid-state NMR spectra (9.4 T) of FFA confined within MCF.

In conclusion, we have demonstrated that ^{19}F NMR spectroscopy can distinguish between molecules of the model pharmaceutical compound present in the pores in confined crystalline and confined amorphous form and a highly mobile species in the form of a molecular-liquid-like layer at the silica surface. To the best of our knowledge, this is the first direct experimental evidence for the presence of a liquid-like layer of molecules on the silica surface. Simultaneous quantification of the three environments allowed us to use ^{19}F solid-state NMR spectroscopy to monitor the kinetics of the confined crystallization in situ. All of the presented studies allowed us to gain a better understanding of the fundamental processes of molecular aggregation at the nanoscale. Considering that 25 % of all marketed drugs are fluorinated molecules,[10] these findings offer a fast and direct diagnostic method for developing novel nanoconfined pharmaceutical formulations.

Acknowledgements

Financial support from the University of East Anglia and the EPSRC Directed Assembly Network is gratefully acknowledged. We are grateful for financial support from the University of East Anglia through a fully funded Ph.D. studentship for K.P.N., and an EPSRC CASE studentship

funded by the EPSRC and Bristol-Myers Squibb to L.E.H. (EP/I501517/1). J.S. and J.A.Z. acknowledge financial support from the EPSRC (EP/J007803/1). We are grateful for having access to the EPSRC funded UK 850 MHz high-field solid-state NMR facility.

Keywords: drug delivery · flufenamic acid · mesoporous silica · nanocrystals · solid-state NMR spectroscopy

How to cite: *Angew. Chem. Int. Ed.* **2016**, *55*, 8904–8908
Angew. Chem. **2016**, *128*, 9050–9054

[1] J. S. Beck, J. C. Vartuli, W. J. Roth, M. E. Leonowicz, C. T. Kresge, K. D. Schmitt, C. T. W. Chu, D. H. Olson, E. W. Sheppard, S. B. McCullen, J. B. Higgins, J. L. Schlenker, *J. Am. Chem. Soc.* **1992**, *114*, 10834–10843.

[2] a) J. T. A. Jones, C. D. Wood, C. Dickinson, Y. Z. Khimyak, *Chem. Mater.* **2008**, *20*, 3385–3397; b) C. Vercaemst, M. Ide, P. V. Wiper, J. T. A. Jones, Y. Z. Khimyak, F. Verpoort, P. Van Der Voort, *Chem. Mater.* **2009**, *21*, 5792–5800; c) K. K. Sharma, T. Asefa, *Angew. Chem. Int. Ed.* **2007**, *46*, 2879–2882; *Angew. Chem.* **2007**, *119*, 2937–2940; d) S. Giret, M. Wong Chi Man, C. Carcel, *Chem. Eur. J.* **2015**, *21*, 13850–13865; e) A.-H. Lu, J.-J. Nitz, M. Comotti, C. Weidenthaler, K. Schlichte, C. W. Lehmann, O. Terasaki, F. Schüth, *J. Am. Chem. Soc.* **2010**, *132*, 14152–14162; f) Z. Y. Zhao, J. Liu, M. Hahn, S. Qiao, A. P. J. Middelberg, L. He, *RSC Adv.* **2013**, *3*, 22008–22013; g) Y. J. Wang, F. Caruso, *Chem. Mater.* **2005**, *17*, 953–961; h) M. Vallet-Regi, F. Balas, D. Arcos, *Angew. Chem. Int. Ed.* **2007**, *46*, 7548–7558; *Angew. Chem.* **2007**, *119*, 7692–7703.

[3] a) J. M. Ha, J. H. Wolf, M. A. Hillmyer, M. D. Ward, *J. Am. Chem. Soc.* **2004**, *126*, 3382–3383; b) B. D. Hamilton, M. A. Hillmyer, M. D. Ward, *Cryst. Growth Des.* **2008**, *8*, 3368–3375; c) B. D. Hamilton, I. Weissbuch, M. Lahav, M. A. Hillmyer, M. D. Ward, *J. Am. Chem. Soc.* **2009**, *131*, 2588–2596; d) Q. Jiang, M. D. Ward, *Chem. Soc. Rev.* **2014**, *43*, 2066–2079; e) B. D. Hamilton, J.-M. Ha, M. A. Hillmyer, M. D. Ward, *Acc. Chem. Res.* **2012**, *45*, 414–423; f) S. Shimizu, K. V. Agrawal, M. O'Mahony, L. W. Drahushuk, N. Manohar, A. S. Myerson, M. S. Strano, *Langmuir* **2015**, *31*, 10113–10118; g) L. M. Dwyer, V. K. Michaelis, M. O'Mahony, R. G. Griffin, A. S. Myerson, *CrystEngComm* **2015**, *17*, 7922–7929.

[4] K. P. Nartowski, J. Tedder, D. E. Braun, L. Fabian, Y. Z. Khimyak, *Phys. Chem. Chem. Phys.* **2015**, *17*, 24761–24773.

[5] a) M. Van Speybroeck, V. Barillaro, T. D. Thi, R. Mellaerts, J. Martens, J. Van Humbeeck, J. Vermant, P. Annaert, G. Van den Mooter, P. Augustijns, *J. Pharm. Sci.* **2009**, *98*, 2648–2658; b) R. Mellaerts, C. A. Aerts, J. Van Humbeeck, P. Augustijns, G. Van den Mooter, J. A. Martens, *Chem. Commun.* **2007**, 1375–1377.

[6] a) F. Babonneau, L. Camus, N. Steunou, A. Ramila, M. Vallet-Regi in *Self-Assembled Nanostructured Materials*, *Vol. 775* (Eds.: Y. Lu, C. J. Brinker, M. Antonietti, C. Bai), Materials Research Society, Warrendale, Pennsylvania, USA, **2003**, pp. 77–82; b) F. Babonneau, L. Yeung, N. Steunou, C. Gervais, A. Ramila, M. Vallet-Regi, *J. Sol-Gel Sci. Technol.* **2004**, *31*, 219–223; c) T. Azais, C. Tourne-Peteilh, F. Aussenac, N. Baccile, C. Coelho, J.-M. Devoisselle, F. Babonneau, *Chem. Mater.* **2006**, *18*, 6382–6390; d) T. Azais, G. Hartmeyer, S. Quignard, G. Laurent, C. Tourne-Peteilh, J.-M. Devoisselle, F. Babonneau, *Pure Appl. Chem.* **2009**, *81*, 1345–1355; e) T. Azais, G. Hartmeyer, S. Quignard, G. Laurent, F. Babonneau, *J. Phys. Chem. C* **2010**, *114*, 8884–8891; f) E. Skorupska, A. Jeziorna, P. Paluch, M. J. Potrzebowski, *Mol. Pharm.* **2014**, *11*, 1512–1519.

[7] F. Guenneau, K. Panesar, A. Nossov, M.-A. Springuel-Huet, T. Azaïs, F. Babonneau, C. Tourné-Péteilh, J.-M. Devoisselle, A. Gédéon, *Phys. Chem. Chem. Phys.* **2013**, *15*, 18805–18808.

[8] A. R. Brás, I. M. Fonseca, M. Dionísio, A. Schönhals, F. Affouard, N. T. Correia, *J. Phys. Chem. C* **2014**, *118*, 13857–13868.

[9] a) M. Delle Piane, M. Corno, A. Pedone, R. Dovesi, P. Ugliengo, *J. Phys. Chem. C* **2014**, *118*, 26737–26749; b) M. Delle Piane, S. Vaccari, M. Corno, P. Ugliengo, *J. Phys. Chem. A* **2014**, *118*, 5801–5807; c) A. Gignone, M. Delle Piane, M. Corno, P. Ugliengo, B. Onida, *J. Phys. Chem. C* **2015**, *119*, 13068–13079.

[10] J. Wang, M. Sánchez-Roselló, J. L. Acena, C. del Pozo, A. E. Sorochinsky, S. Fustero, V. A. Soloshonok, H. Liu, *Chem. Rev.* **2014**, *114*, 2432–2506.

[11] E. P. J. Parrott, J. A. Zeitler, *Appl. Spectrosc.* **2015**, *69*, 1–25.

[12] a) J.-M. Ha, B. D. Hamilton, M. A. Hillmyer, M. D. Ward, *Cryst. Growth Des.* **2012**, *12*, 4494–4504; b) J.-M. Ha, B. D. Hamilton, M. A. Hillmyer, M. D. Ward, *Cryst. Growth Des.* **2009**, *9*, 4766–4777; c) M. Alcoutlabi, G. B. McKenna, *J. Phys. Condens. Matter* **2005**, *17*, R461–R524; d) C. L. Jackson, G. B. McKenna, *Chem. Mater.* **1996**, *8*, 2128–2137; e) V. López-Mejías, J. W. Kampf, A. J. Matzger, *J. Am. Chem. Soc.* **2012**, *134*, 9872–9875.

[13] J. S. Melinger, S. S. Harsha, N. Laman, D. Grischkowsky, *JOSA B* **2009**, *26*, A79–A89.

[14] a) D. V. Nickel, S. P. Delaney, H. Bian, J. Zheng, T. M. Korter, D. M. Mittleman, *J. Phys. Chem. A* **2014**, *118*, 2442–2446; b) N. Y. Tan, J. A. Zeitler, *Mol. Pharm.* **2015**, *12*, 810–815.

[15] J. W. Emsley, L. Phillips, *Prog. Nucl. Magn. Reson. Spectrosc.* **1971**, *7*, 1–526.

Received: March 24, 2016
Revised: May 5, 2016
Published online: June 7, 2016

